Inorganic Chemistry

Article

pubs.acs.org/IC

An Acentric Calcium Borate $Ca_2[B_5O_9]\cdot(OH)\cdot H_2O$: Synthesis, Structure, and Nonliner Optical Property

Qi Wei,[†] Jian-Wen Cheng,*[,‡] Chao He,[†] and Guo-Yu Yang*[,†,§]

[†]State Key Laboratory of Structural Chemistry, Fujian Institute of Research on the Structure of Matter, Chinese Academy of Sciences, Fuzhou, Fujian 350002, China

[‡]Key Laboratory of the Ministry of Education for Advanced Catalysis Materials, Institute of Physical Chemistry, Zhejiang Normal University, Jinhua, Zhejiang 321004, China

[§]MOE Key Laboratory of Cluster Science, School of Chemistry, Beijing Institute of Technology, Beijing 100081, China

Supporting Information

ABSTRACT: A novel noncentrosymmetric calcium borate, $Ca_2[B_5O_9]\cdot(OH)\cdot H_2O$ (**1**), was synthesized under solvothermal condition using mixed solvents of pyridine and H_2O. Compound **1** crystallizes in the monoclinic space group *Cc*. Its structure contains $[B_5O_{12}]$ units and features a three-dimensional (3D) *pcu* net with nine-membered ring (9-MR) channels along the *b*-axis, where the Ca^{2+} cations, OH^- ions, and H_2O molecules are located. Each Ca polyhedron shares three edges and one vertex with four neighbors to form a 3D *dia* Ca−O network. The *pcu* B−O net and *dia* Ca−O net are further interpenetrated to give the final denser net. The second harmonic generation (SHG) measurement shows that compound **1** is a type I phase-matchable material with a strong SHG response of ∼3 times that of KH_2PO_4. In addition, it exhibits a wide transparency range with a short UV cutoff edge below 200 nm. These results reveal that the compound is a potential deep-UV nonlinear optical material. The Vienna ab initio theoretical studies indicate the good SHG response is derived from the synergistic effect of the π-conjugated systems of BO_3 groups and distorted CaO_9 polyhedra.

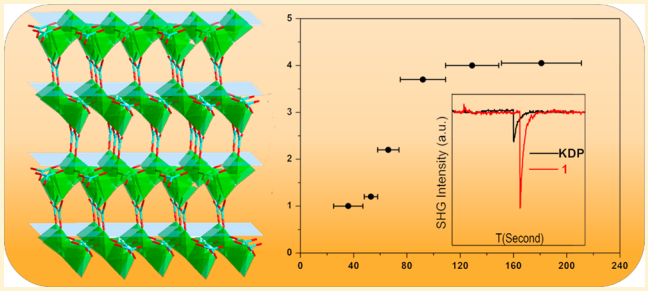

INTRODUCTION

Nonlinear optical (NLO) materials have been of great interest due to their applications in photonic technologies.[1,2] As a remarkable source of NLO materials, borates tend to have wide ultraviolet (UV) transmittance, high second-harmonic generation (SHG) coefficients, and outstanding optical damage thresholds, and these factors make them very attractive for NLO applications in UV and deep-UV regions. Currently, β-BaB_2O_4 (BBO)[2a] and LiB_3O_5 (LBO)[2b] are the two most widely used NLO materials in the UV region. According to Chen's anionic group theory,[3] the large SHG response of BBO and LBO may result from inorganic π-orbital systems of $(B_3O_6)^{3-}$ and $(B_3O_7)^{5-}$ rings. Furthermore, alkali metal and alkaline earth metal−oxygen bonds are favorable for the transmission of UV light because there are no *d*−*d* electron transitions in this region.

Borates show rich structural chemistry; polyborate anions from $[B_3O_3(OH)_4]^-$ to $[B_{18}O_{36}]^{18-}$ have been reported via corner- and/or edge-sharing oxygen atoms of BO_3 triangles and BO_4 tetrahedra.[4,5] The combination of rich oxo boron clusters with alkali/alkaline earth metal ions have produced a variety of UV NLO materials through different synthetic approaches. For example, Pan, Ye, and co-workers successfully obtained a series of alkali metal and alkaline earth metal borates with second-order NLO properties via high-temperature solid-state reaction;[6,7] Belokoneva, Kolis, and co-workers systematically investigated the alkali metal and alkaline earth metal borates and prepared a variety of acentric structure types using hydrothermal method.[8,9] In addition, the incorporation of the alkali/alkaline earth metal cations and halide anions into the borate system led to a series of deep-UV materials with strong SHG response.[10,11]

The properties of NLO materials are also affected by the alkali/alkaline earth metal cations. $KBe_2BO_3F_2$ (KBBF) is a deep-UV NLO crystal and has excellent SHG properties.[2d,e] However, the KBBF crystal suffers a strong layering tendency and high toxicity of beryllium, which severely limits the coherent light output power and commercial availability. Recently, a new beryllium-free deep-UV borate, $Li_4Sr(BO_3)_2$,[12] which preserves the structural merits of KBBF, mitigates the layering tendency and enhances the SHG efficiency by more than half of KBBF.

We have focused on the hydro/solvothermal synthesis of borates and made great advances in the systems of organic amines and inorganic cations templated borates.[13,14] Herein, we obtained a new noncentrosymmetic calcium pentaborate, $Ca_2[B_5O_9]\cdot(OH)\cdot H_2O$, which exhibits a strong SHG response

Received: August 21, 2014
Published: October 15, 2014

   dx.doi.org/10.1021/ic502044d | *Inorg. Chem.* 2014, 53, 11757−11763

of ~3 times that of KH_2PO_4 (KDP) and a wide transparency range with a short UV cutoff edge below 200 nm.

EXPERIMENTAL SECTION

Synthesis. The starting materials are analytical grades and used as purchased without further purification. A mixture of H_3BO_3 (10.0 mmol, 0.614 g), $Ca(OH)_2$ (2.4 mmol, 0.177 g), and Li_2CO_3(1.2 mmol, 0.090 g) was added to the mixed solvents of pyridine (2.0 mL) and H_2O (5.0 mL); the resulting mixture was stirred for ~1.5 h, and the final solution (pH_s = 8–9) was sealed in a 30 mL Teflon-lined stainless steel autoclave, heated at 230 °C for 6 d under autogenous pressure, and then cooled to room temperature (pH_e = 7). Colorless blocklike crystals were obtained (yield 80% based on Ca). It should be stressed that the title compound could not be obtained in the absence of Li_2CO_3; although Li_2CO_3 is not incorporated into the final structure, it may act as a mineralizer in the reaction systems.

Structural Determination. Single-crystal X-ray diffraction (XRD) data were collected on an SCXmini CCD graphite-monochromated with Mo Kα radiation (λ = 0.710 73 Å) at 293 K. The data reduction was done by the program CrystalClear. Multiscan method was used for the absorption correction.[15a] The average structure was solved by direct methods and refined by a full-matrix least-squares fitting on F^2 using SHELXTL-97 program.[15b,c] In the structure, anisotropic displacement parameters were refined for all atomic sites except those of H atoms. The H atoms were geometrically placed and refined using a riding model. The Flack parameter was refined to be 0.00(6), indicative of the correctness of the absolute structure. The structure was verified using the ADDSYM algorithm from the program PLATON,[16] and no higher symmetry was found. Crystal data and structure refinement information are summarized in Table 1, and the selected bond lengths are listed in Table S1 in the Supporting Information.

Table 1. Crystal Data and Structure Refinement for 1

empirical formula	$Ca_2[B_5O_9]\cdot(OH)\cdot H_2O$
formula weight	313.23
temperature	293(2) K
wavelength	0.710 73 Å
crystal system	monoclinic
space group	*Cc*
unit cell dimensions	a = 10.790(5)Å
	b = 6.5174(18)Å
	c = 12.359(6) Å
	β = 114.975(19)°
volume	787.8(6) Å^3
Z, calculated density	4, 2.641 Mg/m^3
absorption coefficient	1.509 mm^{-1}
F(000)	624
crystal size	0.21 × 0.20 × 0.18 mm^3
limiting indices	$-14 \le h \le 14$, $-8 \le k \le 8$, $-16 \le l \le 15$
refletions collected/unique	3006/1537[R(int) = 0.0512]
completeness to θ = 27.47	99.9%
refinement method	full-matrix least-squares on F^2
data/restraints/parameters	1537/8/163
goodness-of-fit on F^2	1.069
final R indices [$I > 2\sigma(I)$]	$R1^a$ = 0.0463, $wR2^a$ = 0.1168
R indices (all data)	$R1^a$ = 0.0509, $wR2^a$ = 0.1220
absolute structure parameter	0.00(6)
largest diff. peak and hole	0.615 and −0.589 e·Å^{-3}

$^a R_1 = \sum||F_0| - |F_c||/\sum|F_0|$, $wR_2 = \{\sum w[(F_0)^2 - (F_c)^2]^2/\sum w[(F_0)^2]^2\}^{1/2}$

Powder X-ray Diffraction and Thermal Analysis. XRD patterns of polycrystalline material were collected on a Rigaku MiniFlex II diffractometer using Cu Kα radiation (λ = 1.540 598 Å) at room temperature in the angular range of 2θ = 5–60° with a step size of 0.02°. The thermogravimetric analysis (TGA) was performed in an air atmosphere with a heating rate of 10 °C/min using a METTLER TGA/SDTA 851^e thermal analyzer.

Infrared and UV–vis–NIR Diffuse Reflectance Spectra. The IR spectrum was obtained on an ABB Bomen MB 102 series Fourier transform infrared (FTIR) spectrophotometer as KBr pellets in the range of 4000–500 cm^{-1}. The optical diffuse reflectance spectrum was measured at room temperature using a PerkinElmer Lambda 900 UV–vis–NIR (NIR = near-infrared) spectrophotometer equipped with an integrating sphere attachment. $BaSO_4$ plate was used as a standard (100% reflectance). The absorption spectrum was calculated from reflectance spectrum using the Kubelka–Munk function: $F(R) = \alpha/S = (1 - R)^2/2R$, where α is the absorption coefficient, S is the scattering coefficient (which is practically wavelength-independent when the particle size is larger than 5 μm), and R is the reflectance.[17]

Second-Order NLO Measurements. The SHG response was measured on powdered samples by using the experimental method adapted from that reported by Kurtz and Perry.[18] 1064 nm radiation generated by a Q-switched Nd:YAG solid-state laser was used as the fundamental frequency light. The samples were ground and sieved into six distinct particle size ranges: 24–48, 48–58, 58–75, 75–109, 109–150, and 150–212 μm, which were pressed into a disk with diameter of 8 mm that was put between glass microscope slides and secured with tape in a 1 mm thick aluminum holder. Sieved of the standard nonlinear optical material KDP samples were used as the reference in identical fashion.

Computational Descriptions. The electronic band structures, density of states, and optical properties were calculated by Vienna Ab Initio Simulation Package (VASP).[19a] The projected augmented wave (PAW)[19b] method with the Perdew–Burke–Ernzerh (PBE)[19c]-type exchange-correlation function was adopted. The plane-wave cutoff energy of 450 eV and the threshold of 10^{-3} eV were set for the self-consistent field convergence of the total electronic energy. In these atoms, H: $1s^1$, B: $2s^22p^1$, O: $2s^22p^4$, Ca: $3p^64s^2$ were treated as valence electrons. The integration of the Brillouin zone was performed by a 4 × 4 × 4 k-point grid sampling for density of states, and the Fermi level (E_f = 0 eV) was selected as the reference.

About 160 empty bands were used in optical property calculations, the scissors operators of 0.16 eV and the 4 × 3 × 3 k-point grids were adopted. The static and dynamic second-order nonlinear susceptibilities $\chi^{abc}(-2\omega;\omega,\omega)$ were calculated based on the length-gauge formalism by Aversa and Sipe.[20] The imaginary part of the static second-order optical susceptibility can be expressed as

$$\chi^{abc} = \frac{e^3}{4h^2\Omega}\sum_{nml,k}\frac{r^a_{nm}(r^b_{ml}r^c_{ln} + r^c_{ml}r^b_{ln})}{2\omega_{nm}\omega_{ml}\omega_{ln}}[\omega_n f_{ml} + \omega_m f_{ln} + \omega_l f_{nm}] + \frac{ie^3}{4h^2\Omega}\sum_{nm,k}\frac{f_{nm}}{\omega^2_{mn}}[r^a_{nm}(r^b_{mn;c} + r^c_{mn;b}) + r^b_{nm}(r^a_{mn;c} + r^c_{mn;a}) + r^c_{nm}(r^a_{mn;b} + r^b_{mn;a})]$$

where r is the position operator, m, n, and l are different band indices, $\hbar\omega_{nm} = \hbar\omega_n - \hbar\omega_m$ is the energy difference for the bands m and n. To better understand the contribution of different states to the susceptibility, the value of m and n could be tuned in our program to include some special bands.

RESULTS AND DISCUSSION

Synthesis. We performed a series of experiments with varied ratios of reagents and different temperatures. When the reaction conditions were changed, another compound, $Ca_2[B_5O_8(OH)]_2[B(OH)_3]\cdot H_2O$ (**2**), was obtained. Compound **2** is isostructural with veatchite-1M, $Sr_2B_{11}O_{16}(OH)_5\cdot H_2O$, which was reported by Grice et al.[21] It was formed in a relatively low temperature with a different reactant ratio than that of **1**. **1** was made with composition of $H_3BO_3/Ca(OH)_2/Li_2CO_3$ in a molar ratio of 25:6:3 under the condition of

dx.doi.org/10.1021/ic502044d | Inorg. Chem. 2014, 53, 11757–11763

230 °C for 6 d, while **2** was made via reaction of H_3BO_3/$Ca(OH)_2$ with a ratio of 7:1 in pyridine (2.0 mL)−H_2O (3.0 mL) mixed solvent under the condition of 190 °C for 5 d. Regretfully, additional attempts for the other alkaline-earth-metal analogues failed.

Description and Discussion of the Structure. Single-crystal X-ray structure analysis revealed that $Ca_2[B_5O_9]\cdot(OH)\cdot H_2O$ (**1**) crystallizes in a noncentrosymmetric monoclinic space group *Cc*. The asymmetric unit of **1** contains one $[B_5O_9]$ cluster, two Ca ions, a hydroxyl group, and a lattice water molecule (Figure S1 in the Supporting Information). The B atoms adopt two kinds of coordination models, namely, BO_3 triangle (Δ) and BO_4 tetrahedron (T). The BO_3 triangles (B1, B4) and BO_4 tetrahedra (B2, B3, B5) have an average B−O distance of 1.367(8) Å and 1.478(7) Å, respectively, which are in good agreement with accepted values of 1.370 and 1.460 Å in the literature.[22] Two BO_3 triangles and three BO_4 tetrahedra are linked via bridging O atoms to give a $[B_5O_{12}]$ unit containing two B_3O_3 rings; the B_3O_3 rings are almost perpendicular to each other.

According to the classification of polyborate anions by Heller,[23a] Christ, and Clark,[23b] $[B_5O_n]$ (n = 10−14) clusters can be classified into five fundamental building blocks (FBBs) with the arrangements of the BO_3 triangles and BO_4 tetrahedra: (5:4Δ+T), (5:3Δ+2T), (5:2Δ+3T), (5:Δ+4T), (5:5T) (Figure 1). The FBBs

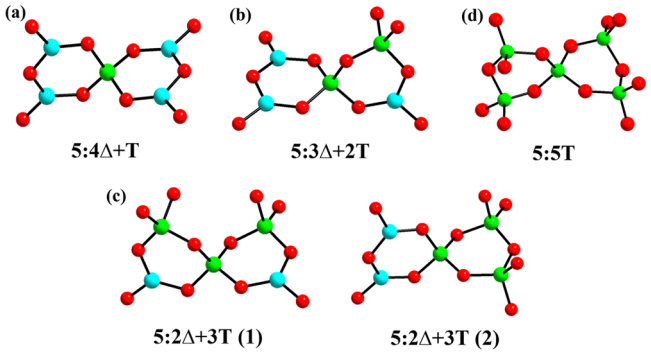

Figure 1. View of known FBBs of $[B_5O_n]$ clusters: (a) B_5O_{10}, 5[(5:4Δ+T)], (b) B_5O_{11}, 5[(5:3Δ+2T)], (c) B_5O_{12}, 5[(5:2Δ+3T)] (2Δ3T:<Δ2T>-<Δ2T> and 2Δ3T:<2Δ*T*>-<3T>), (d) B_5O_{14}, 5[(5:5T)]. Color code: BO_3 (Δ), blue; BO_4 (T), green; O, red (similarly hereinafter).

of (5:4Δ+T) and (5:3Δ+2T) can be further linked with each other to form chains, sheets, and three-dimensional (3D) frameworks with the elimination of water molecules under suitable synthetic conditions.[6a,24] (5:Δ+4T) FBB has never been found in any natural or synthetic borates, while (5:5T) in $H_2InB_5O_{10}$ is the only pentaborate FBB that is constructed solely by BO_4 tetrahedra.[25]

According to the classification of Hawthorne et al.,[22] the (5:2Δ+3T) FBB can be further classified into two types: 2Δ3T:<2Δ*T*>-<3T> and 2Δ3T:<Δ2T>-<Δ2T> (Figure 1c). The former has only been observed in $M_2B_5O_9(OH)$ (M = Sr, Ba),[26] while the latter exists in the structure of $Pb_2B_5O_9I$, which shows an SHG response of ∼13.5 times that of KDP, representing the largest powder NLO coefficient among borates to date.[5c]

The $[B_5O_{12}]$ unit in **1** can be written as 2Δ3T:<Δ2T>-<Δ2T>; each $[B_5O_{12}]$ cluster connects with four neighboring clusters by corner-sharing O atoms to form a 2D-layered structure with a nine-membered ring (9-MR) in the *ab* plane, and these layers are further linked via B−O−B bridges to give a 3D

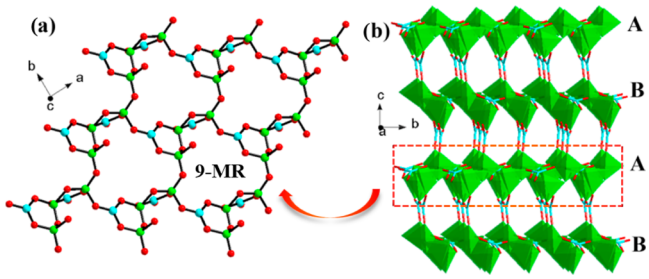

Figure 2. (a) View the layer along *c*-axis. (b) View of the 3D framework featured by the layers with -ABAB- sequence along *a*-axis. Color code: BO_4 tetrahedron, green.

framework along *c*-axis (Figure 2). As shown in Figure 3a, the topology of the 3D framework can be simplified by considering the pentaborate clusters to be six-connected nodes. As a result, a *pcu* topology with the total Schläfli symbol of $\{4^{12}\cdot6^3\}$ is formed.

Compound **1** resembles hilgardite-type[27,28] borates in structural chemistry, in which Cl^- ions are replaced by OH^- groups. The Ca^{2+} and OH^- ions and the H_2O molecules are located at the 9-MR channels along *b*-axis. Two crystallographically independent Ca^{2+} ions are nine-coordinated with distances of 2.344(5)−2.769(4) Å, which is different than eight- and seven-coordinated Ca^{2+} ions in hilgardite $Ca_2B_5O_9Cl\cdot H_2O$[27a] (Figure S2 and Table S1 in the Supporting Information). Bond-valence-sum (BVS) calculations gave total bond valences of 1.978 for Ca1 and 1.877 for Ca2. Besides, the OH group and H_2O molecule were also further identified by BVS calculations (Table S2 in the Supporting Information). The OH^- ions and H_2O molecules interact with the framework O atoms by hydrogen bonding, with O···O distances range from 2.727(6) to 3.547(7) Å. In addition, there is also hydrogen bonding between OH^- and O1W with a distance of 2.580(6) Å (Figure 4a). Each Ca polyhedron shares three edges and one vertex with four neighbors to form a 3D Ca−O framework. The 3D Ca−O network can be described as a four-connected diamond (*dia*) topology with a Schläfli symbol of $\{6^6\}$ (Figure 3b). The *pcu* B−O net and *dia* Ca−O net are further interpenetrated to give a denser net (Figure 3c).

Comparison of 1 with $BaPb[B_5O_9(OH)]\cdot H_2O$. It is worthwhile to compare compound **1** with $BaPb[B_5O_9(OH)]\cdot H_2O$ (Figure 4),[29] since **1a** also crystallizes in space group *Cc* and consists of $[B_5O_{11}(OH)]$ clusters (2Δ3T:<Δ2T>-<Δ2T>). In **1** and BaPb-$[B_5O_9(OH)]\cdot H_2O$, the layers are stacked along the *c*-axis with the triangles arranged into the same side of the layer, which leads to the noncentrosymmetric structures. The adjacent layers in **1** linked together through bridging O atoms to generate a 3D network, while $BaPb[B_5O_9(OH)]\cdot H_2O$ features a 2D anionic network. The structural evolution of $BaPb[B_5O_9(OH)]\cdot H_2O$ to **1** may be due to the different ionic radiuses of cations. The smaller Ca^{2+} ions in **1** (ionic radius: Ca^{2+}/1.06 Å, Ba^{2+}/1.43 Å, Pb^{2+}/1.32 Å) make the distance between two adjacent layers shorter (6.40 Å) than that in **1a** (8.96 Å). The shorter interactions can draw the NLO-active anionic groups closer to each other forming a denser packing and increase the density of the active groups, which tend to produce a larger NLO effect. A similar cation effect has been found in $LiNa_5Be_{12}B_{12}O_{33}$,[30a] $ACaCO_3F$,[30b] and $ACd_4Ga_5Se_{12}$[30c] (A = K, Rb, Cs). The terminal hydroxyls of BO_4 tetrahedron in **1a** point into the layer; the longer distance of adjacent layers prevents the single layer further connected into 3D network by condensation

dx.doi.org/10.1021/ic502044d | *Inorg. Chem.* 2014, 53, 11757−11763

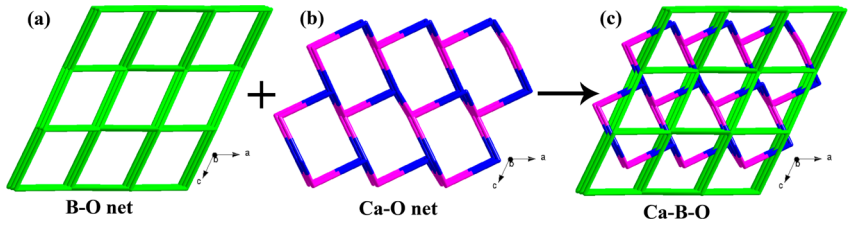

Figure 3. (a) View of the *pcu* B−O net. (b) View of the *dia* Ca−O net. (c) The interpenetrated *pcu* B−O net and *dia* Ca−O net in **1**. Color code: green, $[B_5O_{12}]$ nodes; fuchsia/blue, CaO_9 nodes.

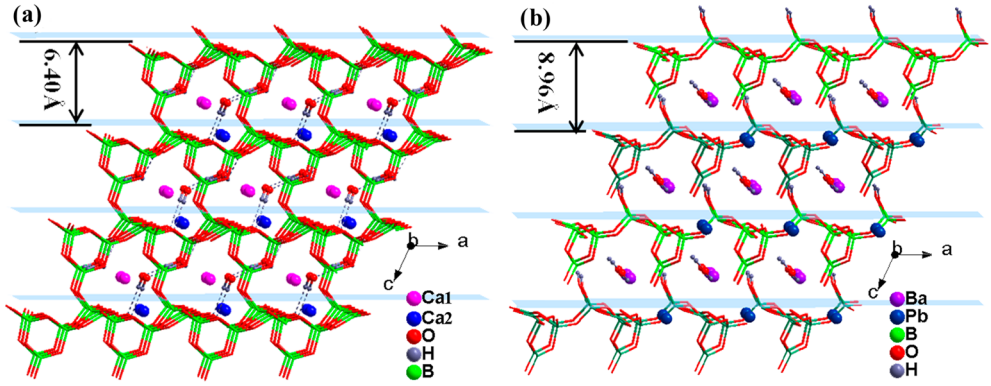

Figure 4. (a) View of the 3D $Ca_2[B_5O_9]\cdot(OH)\cdot H_2O$ with 9-MR channels along *b*-axis. (b) View of the 2D $BaPb[B_5O_9(OH)]\cdot H_2O$ along *b*-axis.

reactions with the elimination of water molecules, while the hydroxyl groups in **1** locate inside the 9-MRs (Figure 4a). A similar reaction that used other alkaline-earth-metal ions could not produce the isomorphous products of **1**, indicating the suitable size of Ca^{2+} ion is indeed critical for the formation of structure.

Physical Characterization. The experimental powder X-ray diffraction (PXRD) pattern of **1** matches well with the simulated PXRD pattern; the difference in reflection intensities between the simulated and the experimental patterns was due to the variation in the preferred orientation of the powder sample during collection of the experimental PXRD data (Figure S3 in the Supporting Information). The thermal behavior of **1** was examined by the thermogravimetric analysis (TGA) in dry-air atmosphere (Figure S4 in the Supporting Information). TGA shows that **1** has a two-step weight loss; the minor weight loss of 0.53% from 30 to 95 °C is due to surface moisture of the sample. Above this temperature to 520 °C, the weight loss is about 9.0%, which corresponds to the loss of 1.5 water molecules (calcd 8.62%). The weight loss between 520 and 1000 °C might be attributed to the gradual volatilization of boron oxide. Powder XRD analysis indicated that the fundamental packing of **1** remains stable until at least 380 °C. When the polycrystalline sample was heated at 420 °C, its framework started to collapse (Figure S4 in the Supporting Information).

In the IR spectrum of **1**, the broad absorption band around 3549 and 3415 cm^{-1} is assigned to the asymmetric stretching vibrations and symmetric stretching vibrations of O−H bonds. The band at 1645 cm^{-1} is assigned to the H−O−H bending mode, which shows that compound **1** contains water molecule. The characteristic band at ∼1371 cm^{-1} is due to B−O asymmetric stretching of BO_3 units, and the bands around 1067−1116 and 855 cm^{-1} are associated with the asymmetric and symmetric stretching of B−O in BO_4 units, respectively. In addition, the band at 657 cm^{-1} is the out-of plane bending of B−O in BO_3 units (Figure S5 in the Supporting Information). The IR spectrum clearly confirms the presence of OH groups and BO_3 and BO_4 units in **1**, which is consistent with the crystal structure result.

Nonlinear Optical Property. The noncentrosymmetric crystal structure of **1** prompts us to examine its SHG property. SHG measurements on a Q-switched Nd:YAG laser with sieved powder samples revealed that compound **1** exhibits a strong SHG response of ∼3 times that of KDP standard of similar grain size (Figure 5a). In addition, compound **1** is found to be phase-matchable (Figure 5b). On the basis of the anionic group theory[3] of NLO activity in borates, the contribution of BO_4 tetrahedra to the response is small; the strong SHG efficiency may be attributed to the π-conjugated systems of triangular BO_3 groups, which have the asymmetric electronic distributions qualitatively. The UV−vis−NIR diffuse reflectance spectrum of **1** in the region of 200−1400 nm is displayed in Figure 6a. Obviously, it has a cutoff edge below 200 nm, which suggests that compound **1** is a potential deep-UV NLO material. Absorption (K/S) data were calculated from the Kubelka−Munk function:[17] $F(R) = (1-R)^2/2R = K/S$, it reveals that the band gap of **1** is 5.45 eV (Figure S6 in the Supporting Information), which is comparable to those of deep-UV NLO borates[6c,31] such as $Cs_2SiB_4O_9$[31a] and $Li_4Rb_3B_7O_{14}$[31b] (band gaps of 5.21 and 5.51 eV, respectively).

Theoretical Studies. To better understand the structure-property relation and the origin of the SHG response, the electronic band structures were analyzed using the VASP.[19] The band structure of **1** is presented in Figure 6b. For convenience, the Fermi level was shifted to 0 eV when discussing the electronic structures. The top of the valence bands (VBs) is located at A point, and the bottom of the conduction bands is located at G point. So it has an indirect band gap of 5.29 eV, which is smaller than the experimental value of 5.45 eV owing to the underestimation of the band gap by PBE.[19c] And a scissor value of 0.16 eV is applied to the optical property calculation in the following study. The total and partial density

dx.doi.org/10.1021/ic502044d | *Inorg. Chem.* 2014, 53, 11757−11763

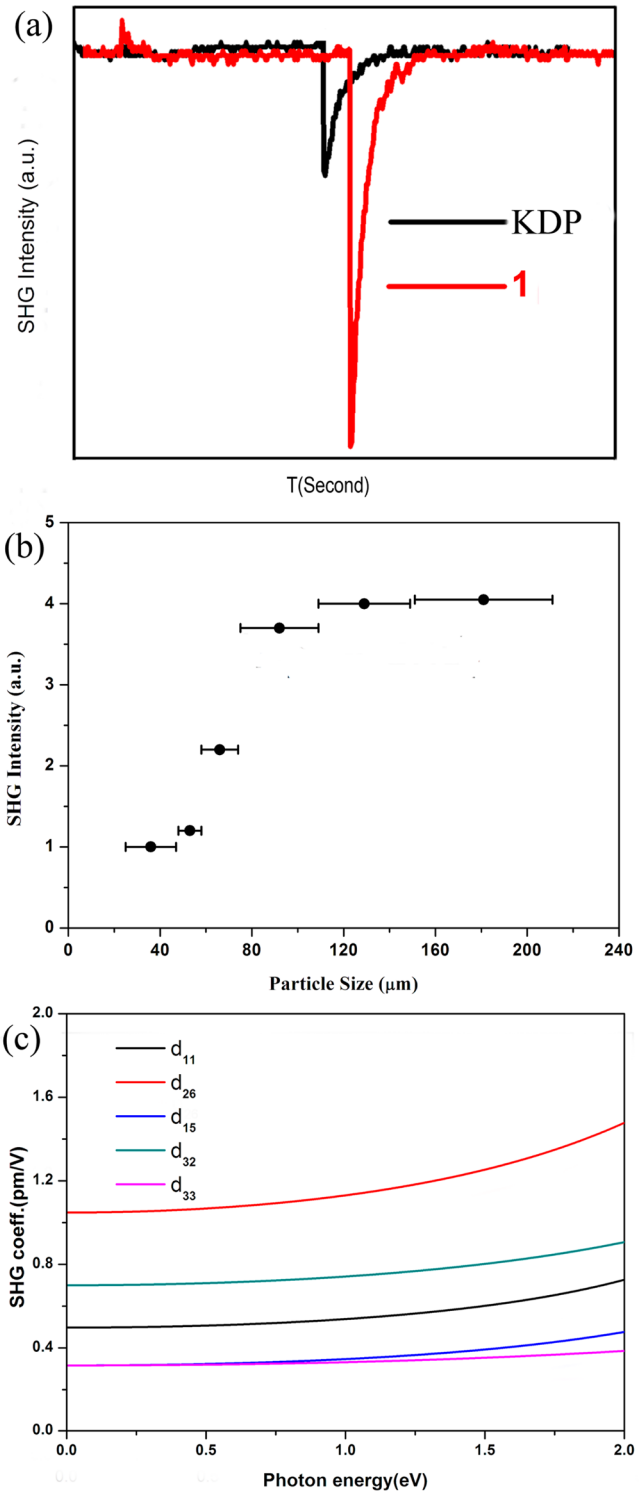

Figure 5. (a) Oscilloscope traces of SHG signals for the powder of **1** and KDP in the same particle size of 109−150 μm. (b) Phase-matching curve of **1** (particle size vs SHG intensity). (c) Calculated frequency-dependent SHG coefficients of **1**.

of states (DOS and PDOS, respectively) are presented in Figure S7 (in the Supporting Information). VBs ranging from −20.63 to −17.14 eV are formed by B 2s, B 2p, O 2s, and Ca 3p hybridized with small amount of H 1s state, while VBs from −8.75 to E_f are mostly contributions of B 2s, B 2p, and O 2p, with small amounts of H 1s state. B 2p with small amounts of O 2p state make up the conduction bands (CBs) between E_f up to 12.38 eV.

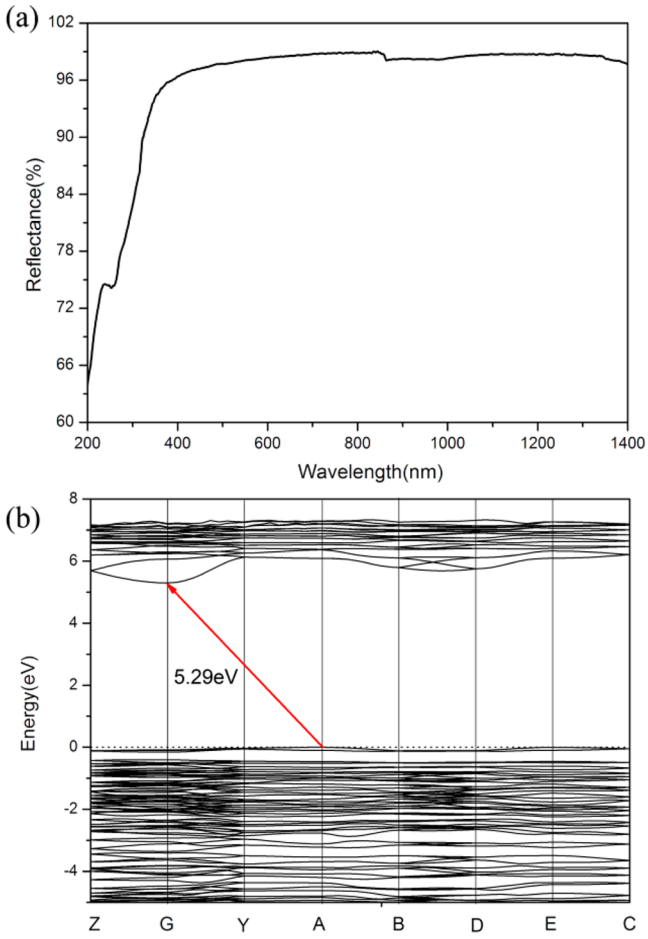

Figure 6. (a) UV−vis−NIR diffuse reflectance spectrum of **1**. (b) Band structures of **1** (The Fermi level is set at 0 eV).

The title compound has 14 nonzero SHG coefficient tensors (d_{11}, d_{12}, d_{13}, d_{15}, d_{16}, d_{21}, d_{23}, d_{24}, d_{26}, d_{31}, d_{32}, d_{33}, d_{34}, and d_{35}), and the frequency-dependent SHG coefficients of the crystal are plotted in Figure 5c. For simplicity, we only list the five largest coefficients. The magnitudes of d_{11}, d_{26}, d_{15}, d_{32}, and d_{33} at 1064 nm (1.165 eV) are presented. The results are in accordance with the experimental value that is approximately related to the effective SHG coefficient. The local structure contributions of the compound to the overall SHG efficiency were estimated by the cutoff-energy-dependent SHG coefficient[5c] according to the length-gauge formalism. As shown in Figure S8 (in the Supporting Information), the states at VB-1, VB-3, VB-5, CB-1, and CB-2 make the most significant contributions to the SHG coefficient. VB-1 is dominated by B 2p hybridized with O-2p, and VB-3 is dominated by B-2s, B-2p, and O-2p. VB-5 is dominated by Ca-3p, O-2s, B-2p, and little B-2s. CB-1 and CB-2 are mainly dominated by B-2p and Ca-3d. So the strong SHG responses are mostly contributions of the π-conjugated systems of triangular BO_3 groups and distorted CaO_9 polyhedra. Additionally, the direction of the dipole moments for $Ca(1/2)O_9$ polyhedra and BO_3 triangles are shown in Supporting Information, Figure S9; clearly, the vector sum magnitudes of these dipole moments is mainly enhanced along *c*-axis, which leads to the good SHG response.

CONCLUSIONS

In summary, a new noncentrosymmetric calcium pentaborate has been synthesized under solvothermal condition using mixed

dx.doi.org/10.1021/ic502044d | *Inorg. Chem.* 2014, 53, 11757−11763

solvent of pyridine and H_2O. The framework of **1** displays a hilgardite-type framework with 9-MR channels. The *pcu* B−O net and *dia* Ca−O net are further interpenetrated to form the final denser net, which is conducive to a larger NLO effect. Compound **1** exhibits a strong SHG response of ∼3 times that of KDP and is phase-matchable. Furthermore, the UV−vis−NIR diffuse reflectance spectrum indicates **1** has a wide transparency range with a short UV cutoff edge below 200 nm. These characteristics make it a potential deep-UV NLO material. Theoretical analyses reveal that the synergistic effect of the π-conjugated systems of BO_3 groups and distorted CaO_9 polyhedra is responsible for the SHG response. Further work is in progress for discovering new UV NLO alkali metal and alkaline earth metal borates under solvothermal conditions.

■ ASSOCIATED CONTENT

Supporting Information

X-ray crystallographic file in CIF format (CSD-426915), selected bond distances, simulated and measured powder XRD patterns, IR spectrum, TGA, theoretical calculations, and additional structures. This material is available free of charge via the Internet at http://pubs.acs.org.

■ AUTHOR INFORMATION

Corresponding Authors

*E-mail: ygy@fjirsm.ac.cn or ygy@bit.edu.cn. (G.-Y.Y.)
*E-mail: jwcheng@zjnu.cn. (J.-W.C.)

Notes

The authors declare no competing financial interest.

■ ACKNOWLEDGMENTS

This work was supported by the NSFC (Nos. 91122028, 20121001, 50872133, and 21471130), the NSFC for Distinguished Young Scholars (No. 20725101), and the 973 program (Nos. 2014CB932101 and 2011CB932504). We also thank Prof. Y. Zhang of Fuzhou University for his technical assistance.

■ REFERENCES

(1) (a) Becker, P. *Adv. Mater.* **1998**, *10*, 979−992. (b) Ok, K. M.; Chi, E. O.; Halasyamani, P. S. *Chem. Soc. Rev.* **2006**, *35*, 710−717.

(2) (a) Chen, C. T.; Wu, B. C.; Jiang, A. D.; You, G. M. *Sci. Sin., Ser. B* **1985**, *28*, 235−243. (b) Chen, C. T.; Wu, Y. C.; Jiang, A. D.; Wu, B. C.; You, G. M.; Li, R. K.; Lin, S. J. *J. Opt. Soc. Am. B* **1989**, *6*, 616−621. (c) Wu, Y. C.; Sasaki, T.; Nakai, S.; Yokotani, A.; Tang, H. G.; Chen, C. T. *Appl. Phys. Lett.* **1993**, *62*, 2614−2615. (d) Chen, C. T.; Xu, Z. Y.; Deng, D. Q.; Zhang, J.; Wong, G. K. L. *Appl. Phys. Lett.* **1996**, *68*, 2930−2932. (e) Chen, C. T.; Ye, N.; Lin, J.; Jiang, J.; Zeng, W. R.; Wu, B. C. *Adv. Mater.* **1999**, *11*, 1071−1078.

(3) (a) Chen, C. T. *Sci. Sin. (Engl. Ed.)* **1979**, *22*, 756−776. (b) Chen, C. T.; Liu, G. *Annu. Rev. Mater. Sci.* **1986**, *16*, 203−243. (c) Chen, C. T.; Wu, Y. C.; Li, R. K. *Int. Rev. Phys. Chem.* **1989**, *8*, 65−91.

(4) (a) Huppertz, H. *Chem. Commun.* **2011**, *47*, 131−140. (b) Wang, S.; Alekseev, E. V.; Depmeierc, W.; Albrecht-Schmitt, T. E. *Chem. Commun.* **2011**, *47*, 10874−10885. (c) Belokoneva, E. L. *Crystallogr. Rev.* **2005**, *11*, 151−198.

(5) (a) Lin, Z. E.; Yang, G. Y. *Eur. J. Inorg. Chem.* **2011**, 3857−3867. (b) Tian, H. R.; Wang, W. H.; Gao, Y. E.; Deng, T. T.; Wang, J. Y.; Feng, Y. L.; Cheng, J. W. *Inorg. Chem.* **2013**, *52*, 6242−6244. (c) Huang, Y. Z.; Wu, L. M.; Wu, X. T.; Li, L. H.; Chen, L.; Zhang, Y. F. *J. Am. Chem. Soc.* **2010**, *132*, 12788−12789.

(6) (a) Wang, Y. J.; Pan, S. L.; Tian, X. L.; Zhou, Z. X.; Liu, G.; Wang, J. D.; Jia, D. Z. *Inorg. Chem.* **2009**, *48*, 7800−7804. (b) Yang, Y.; Pan, S. L.; Li, H. Y.; Han, J.; Chen, Z. H.; Zhao, W. W.; Zhou, Z. X. *Inorg. Chem.* **2011**, *50*, 2415−2419. (c) Wang, L.; Pan, S. L.; Chang, L. X.; Hu, J. Y.; Yu, H. W. *Inorg. Chem.* **2012**, *51*, 1852−1858.

(7) (a) Wang, S. C.; Ye, N.; Li, W.; Zhao, D. *J. Am. Chem. Soc.* **2010**, *132*, 8779−8786. (b) Wang, S. C.; Ye, N. *J. Am. Chem. Soc.* **2011**, *133*, 11458−11461. (c) Zou, G. H.; Ma, Z. J.; Wu, K. C.; Ye, N. *J. Mater. Chem.* **2012**, *22*, 19911−19918.

(8) (a) Belokoneva, E. L.; Dimitrova, O. V. *Inorg. Chem.* **2013**, *52*, 3724−3727. (b) Belokoneva, E. L.; Stefanovich, S. Y.; Dimitrova, O. V. *J. Solid State Chem.* **2012**, *195*, 79−85.

(9) (a) McMillen, C. D.; Stritzinger, J. T.; Kolis, J. W. *Inorg. Chem.* **2012**, *51*, 3953−3955. (b) Heyward, C.; McMillen, C. D.; Kolis, J. W. *Inorg. Chem.* **2012**, *51*, 3956−3962. (c) McMillen, C. D.; Kolis, J. W. *Inorg. Chem.* **2011**, *50*, 6809−6813.

(10) (a) Wu, H. P.; Pan, S. L.; Poeppelmeier, K. R.; Li, H. Y.; Jia, D. Z.; Chen, Z. H.; Fan, X. Y.; Yang, Y.; Rondinelli, J. M.; Luo, H. *J. Am. Chem. Soc.* **2011**, *133*, 7786−7790. (b) Wu, H. P.; Yu, H. W.; Yang, Z. H.; Hou, X. L.; Su, X.; Pan, S. L.; Poeppelmeier, K. R.; Rondinelli, J. M. *J. Am. Chem. Soc.* **2013**, *135*, 4215−4218. (c) Yu, H. W.; Wu, H. P.; Pan, S. L.; Yang, Z. H.; Su, X.; Zhang, F. F. *J. Mater. Chem.* **2012**, *22*, 9665−9670.

(11) (a) Huang, H. W.; Yao, J. Y.; Lin, Z. S.; Wang, X. Y.; He, R.; Yao, W. J.; Zhai, N. X.; Chen, C. T. *Angew. Chem., Int. Ed.* **2011**, *50*, 9141−9144. (b) Huang, H. W.; Yao, J. Y.; Lin, Z. S.; Wang, X. Y.; He, R.; Yao, W. J.; Zhai, N. X.; Chen, C. T. *Chem. Mater.* **2011**, *23*, 5457−5463.

(12) Zhao, S. G.; Gong, P. F.; Bai, L.; Xu, X.; Zhang, S. Q.; Sun, Z. H.; Lin, Z. S.; Hong, M. C.; Chen, C. T.; Luo, J. H. *Nat. Commun.* **2014**, *5*, 4019.

(13) (a) Rong, C.; Yu, Z. W.; Wang, Q.; Zheng, S. T.; Pan, C. Y.; Deng, F.; Yang, G. Y. *Inorg. Chem.* **2009**, *48*, 3650−3659. (b) Cao, G. J.; Lin, J.; Zheng, S. T.; Fang, W. H.; Yang, G. Y. *Dalton Trans.* **2010**, *39*, 8631−8636. (c) Zhou, J.; Fang, W. H.; Rong, C.; Yang, G. Y. *Chem.—Eur. J.* **2010**, *16*, 4852−4863. (d) Wei, L.; Wei, Q.; Lin, Z. E.; Meng, Q.; He, H.; Yang, B. F.; Yang, G. Y. *Angew. Chem., Int. Ed.* **2014**, *53*, 7188−7191. (e) Zhao, P.; Lin, Z. E.; Wei, Q.; Cheng, L.; Yang, G. Y. *Chem. Commun.* **2014**, *50*, 3592−3594.

(14) (a) Wang, G. M.; Sun, Y. Q.; Yang, G. Y. J. *Solid State Chem.* **2006**, *179*, 398−403. (b) Wu, H. Q.; Ju, P.; He, H.; Yang, B. F.; Yang, G. Y. *Inorg. Chem.* **2013**, *52*, 10566−10570. (c) Wei, Q.; Li, L.; Cheng, L.; Meng, Q.; Yang, G. Y. *Dalton Trans.* **2014**, *43*, 9427−9430. (d) Cheng, L.; Wei, Q.; Wu, H. Q.; Zhou, L. J.; Yang, G. Y. *Chem.—Eur. J.* **2013**, *19*, 17662−17667.

(15) (a) *CrystalClear,* version 1.3.5; Rigaku Corp.: The Woodlands, TX, 1999. (b) Sheldrick, G. M. *SHELXTL-97, Program for Solution of Crystal Structures;* University of Göttingen: Germany, 1997. (c) Sheldrick, G. M. *SHELXS-97, Program for Solution of Crystal Refinement;* University of Göttingen: Germany, 1997.

(16) Spek, A. L. *J. Appl. Crystallogr.* **2003**, *36*, 7−13.

(17) Wendlandt, W. M.; Hecht, H. G. *Reflectance Spectroscopy;* Interscience: New York, 1966.

(18) Kurtz, S. K.; Perry, T. T. *J. Appl. Phys.* **1968**, *39*, 3798−3813.

(19) (a) Kresse, G.; Furthmüller, J. *Phys. Rev. B* **1996**, *54*, 11169−11186. (b) Blochl, P. E. *Phys. Rev. B* **1994**, *50*, 17953−17979. (c) Perdew, J. P.; Burke, K.; Ernzerhof, M. *Phys. Rev. Lett.* **1996**, *77*, 3865−3868.

(20) (a) Aversa, C.; Sipe, J. *Phys. Rev. B* **1995**, *52*, 14636−14645. (b) Rashkeev, S. N.; Lambrecht, W. R. L.; Segall, B. *Phys. Rev. B* **1998**, *57*, 3905−3919.

(21) Grice, J. D.; Pring, A. *Am. Mineral.* **2012**, *97*, 489−495.

(22) Hawthorne, F. C.; Burns, P. C.; Grice, J. D. Mineralogical Society of America: Washington, DC, 2002, *33*, 41−115.

(23) (a) Heller, G. A. *Top. Curr. Chem.* **1986**, *131*, 39−98. (b) Christ, C. L.; Clark, J. R. *Phys. Chem. Miner.* **1977**, *2*, 59−87.

(24) (a) Merlino, S.; Sartori, F. *Acta Crystallogr.* **1972**, *B28*, 3559−3567. (b) Merlino, S.; Sartori, F. *Acta Crystallogr.* **1969**, *B25*, 2264−2270. (c) Cannillo, E.; Negro, A. D.; Ungaretti, L. *Am. Mineral.* **1973**, *58*, 110−115. (d) Corazza, E.; Menchetti, S.; Sabelli, C. *Acta Crystallogr.* **1975**, *B31*, 2405−2410.

(25) Cong, R. H.; Yang, T.; Li, H. M.; Liao, F. H.; Wang, Y. X.; Lin, J. H. *Eur. J. Inorg. Chem.* **2010**, *11*, 1703−1709.
(26) McMillen, C.; Heyward, C.; Giesber, H.; Kolis, J. *J. Solid State Chem.* **2011**, *184*, 2966−2971.
(27) (a) Ghose, S.; Wan, C. *Am. Mineral.* **1979**, *64*, 187−195. (b) Ghose, S. *Am. Mineral.* **1982**, *67*, 1265−1272.
(28) (a) Burns, P. C.; Hawthorne, F. C. *Acta Crystallogr.* **1994**, *C50*, 653−655. (b) Barbier, J.; Park, H. *Can. Miner.* **2001**, *39*, 129−135. (c) Ferro, O.; Merlino, S.; Vinogradova, S. A.; Pushcharovsky, D. Yu.; Dimitrova, O. V. *J. Alloys Compd.* **2000**, *305*, 63−71.
(29) Wu, H. Q.; He, H.; Yang, B. F.; Yang, G. Y. *Inorg. Chem. Commun.* **2013**, *37*, 77−79.
(30) (a) Huang, H. W.; Liu, L. J.; Jin, S. F.; Yao, W. J.; Zhang, Y. H.; Chen, C. T. *J. Am. Chem. Soc.* **2013**, *135*, 18319−18322. (b) Zou, G. H.; Ye, N.; Huang, L.; Lin, X. S. *J. Am. Chem. Soc.* **2011**, *133*, 20001−20007. (c) Lin, H.; Chen, L.; Zhou, L. J.; Wu, L. M. *J. Am. Chem. Soc.* **2013**, *135*, 12914−12921.
(31) (a) Wu, H. P.; Yu, H. W.; Pan, S. L.; Huang, Z. J.; Yang, Z. H.; Su, X.; Poeppelmeier, K. R. *Angew. Chem., Int. Ed.* **2013**, *52*, 3406−3410. (b) Zhang, B. B.; Yang, Z. H.; Yang, Y.; Lee, Mi. H.; Pan, S. L.; Jing, Q.; Su, X. *J. Mater. Chem. C* **2014**, *2*, 4133−4141.